Proceedings of the 9th International Symposium on
Dynamics and Control of Process Systems (DYCOPS 2010),
Leuven, Belgium, July 5-7, 2010
Mayuresh Kothare, Moses Tade, Alain Vande Wouwer, Ilse Smets (Eds.)

WeET4.3

Modeling of Gate Control Neuronal Circuitry Including Morphologies and Physiologies of Component Neurons and Fibres

Egemen Agi*. Canan Ozgen **
Nuhan Purali***

*Middle East Technical University, Ankara ,06531
TURKEY (Tel: 905366499252; e-mail: e133873@ metu.edu.tr).
** Middle East Technical University, Ankara ,06531 TURKEY (e-mail:
cozgen@metu.edu.tr)
*** Biophysics Department, Medical School of Hacettepe University,
Ankara, TURKEY, (e-mail: npurali@hacettepe.edu.tr)

Abstract: In this work mathematical model of gate control theory, which explains the modulation of pain signals with tactile signals, is done. The difference of the current developed model from the previous modeling trials is that electrophysiological and morphological properties of component neurons and fibers that constitute the gate control structure are included to observe the structure-function relationship. Model of a single excitable cell is used as the main building block of the models of one unmyelinated fiber, one myelinated fiber, one interneuron and one projection neuron. The conduction velocities in the unmyelinated and myelinated fibers are found as 0.43m/s and 64.35 m/s, respectively. For both fibers input current intensity-frequency relationships are constructed. In addition, synapses between neurons are developed as two independent tanks and developed synapse model exhibits the summation and tetanization properties of real synapses while simulating the time dependency of neurotransmitter concentration in the synaptic cleft. All of the individual parts of the gate control system are connected and the whole system is simulated for different connection configurations.

Keywords: Action potential, Hodgkin-Huxley model, ion channels, synaptic transmission, substantia gelatinosa.

1. INTRODUCTION

Control mechanisms in living organisms are very stable and robust and thus worth investigation from an engineering perspective. These control mechanisms can be imitated and applied in engineering sciences. Also theories existing for engineering purposes can be utilized to fix any malfunction in the system. Consequently, the engineering theories can be utilized in the field of nano-medicine.

One of the control mechanisms in a living organism is the gate control, which modulates the pain signals. In the treatment of chronic pain, electrical stimulation of spinal cord is used which imbeds gate control system [1]. In order to increase the efficiency of this method and to find the possible target points for pain killer drugs, the mechanism of suppression of pain has to be studied thoroughly.

Neuronal structure of the gate control mechanism is very simple. However, due to high heterogeneity in the electrophysiological and morphological characteristics of neurons, formulation of the circuit from the exact neurons is extremely complex. In recent years, connectivity patterns between neurons that are most probable to be included in gate control mechanism are investigated to find exact circuits that process pain signaling. Also, morphological and electrophysiological properties of these neurons are investigated to find their signaling properties [2].

Previous models of gate control structure did not take into account the physiological and morphological properties of the components of the system. They were either phenomenological models in which signal initiation is modeled without regarding the biophysics behind the process [3] or black box models that use artificial neural networks using only input and output data without any first principal models [4].

The aim of the current study is to model gate control theory considering morphological and electrophysiological properties of the neurons.

2. GATE CONTROL STRUCTURE

Gate control theory was proposed by Melzack and Wall in 1965 [5]. In their work, level of pain that was perceived was determined by the activity difference between the unmyelinated fibers and myelinated fibers. Myelin is an insulating cover that reduces the capacitance of the membrane and increases the membrane resistance. In Fig.1 schematic of the gate control structure is shown. Output of transmission cells (T-cells) determines the level of pain. In this structure unmyelinated fiber (C fiber) carries the

nociceptive (pain related) signals and it tries to excite transmission cell and inhibit the SG neuron (substantia gelatinosa neuron). SG neuron inhibits T-cell so by this way unmyelinated fiber decreases the inhibitory effect of interneuron on the transmission cell. Myelinated fiber (Aβ) carries non-nociceptive signals and excites both the interneuron and the transmission cell. By exciting interneuron, myelinated fiber increases the inhibitory effect of interneuron on the transmission cell. The activity difference between the unmyelinated and myelinated fibers determines the firing rate of transmission cell which determines the level of perceived pain.
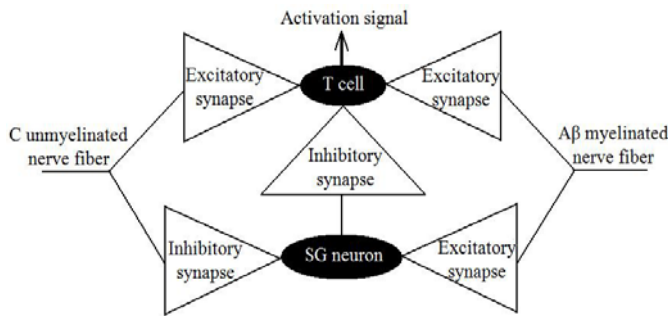
Fig.1. Schematic of gate control structure.

Melzack and Wall did not state the exact place of the transmission cells in their work [5], however, Wall gave the neurons of lamina I and lamina V of the dorsal horn of the spinal cord as candidates for being the transmission cells [16]. In the most recent papers lamina I neurons are associated with nociception and are stated to be projection neurons that send nociceptive signals to brain through ascending pathways [8, 9, 10]. So in the current work lamina I cells are treated to be transmission cells. Substantia gelatinosa neurons are situated in the lamina II of the dorsal horn.

There is not one kind of neuron neither in substantia gelatinosa nor in marginal zone. Neurons of these layers differ morphologically and also with their response to same stimuli. Tonic cells in lamina I are chosen as the transmission cells since they were reported to tend to integrate incoming inputs [8]. In addition they were reported to be able to transduce stimulus intensity into firing frequency [8]. Tonic cells fire action potentials continuously with a constant frequency as long as the stimuli sustains. When the firing characteristics and morphology of the cells are explored, it is found that tonic cells correspond to fusiform cells [8]. Fusiform cells are identified with their elongated soma and primary dendrites arising from each end of the soma [11] which means they have two primary dendrites [8]. In the work of Han et.al. responses of cat lamina I neurons were recorded and it was found that all of the fusiform cells that were labeled were nociceptive specific [12] which is another reason why fusiform cells may be chosen as T-cells in gate control system.

Interneuron should possess inhibitory neurotransmitter so that it can inhibit transmission cell. When the cell groups in lamina II were investigated, islet cells were found to be immunoreactive for γ-aminobutyric acid (GABA) which is the main inhibitory neurotransmitter in superficial dorsal horn [13]. In the work of Maxwell et.al., it is stated that islet cells had axons that project outside the territory of dendritic tree which made them great candidates for being inhibitory interneurons since they may collect information from one sensory region and inhibit other neurons outside this region [14]. Under sustained depolarization islet cells generate action potentials tonically and this electrophysiological property is stated to be consistent with an inhibitory function [14]. In the light of these data, an islet cell is used as the interneuron in the gate control structure.

3. MODELING STUDIES

3.1 Single Excitable Cell

For the model of single excitable cell Hodgkin-Huxley formalism is used. Hodgkin and Huxley modeled the cell membrane as an electrical circuit [15] as in Fig.2 and explained the formation of action potential which is the unit signal in the nervous system.
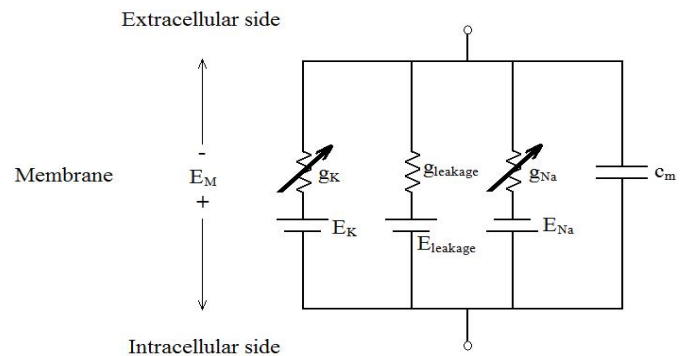
Fig.2. Equivalent electrical circuit of excitable cell membrane.

The cell membrane is composed of voltage-gated sodium and potassium channels whose conductance change with membrane voltage, leakage channels, which have constant conductance, and membrane capacitance. Potassium voltage gated channels have four activating particles whereas sodium channels possess three activating, one inactivating channels. Activating particles open with increasing membrane voltage and inactivating particles close with increasing membrane voltage. All of the particles have two states; open and closed states and transition between these states is modeled with first order reaction kinetics as in Eq.1.

$$1 - x \underset{\beta_x}{\overset{\alpha_x}{\leftrightarrow}} x \qquad (1)$$

In Eq.1 three different variables can be written in place of x; n, probability of potassium activating particles to be in open state, m, probability of sodium activating particles to be in open state and h, probability of sodium inactivating particles to be in open state. α_x and β_x are the forward and backward rate constants, respectively, and they are voltage dependent. Dynamics of voltage gated ion channels are based on the work of Schwarz et.al. [16] with some alterations. First, sodium current is calculated with an ohmic relation instead of

Goldman-Hodgkin-Katz (GHK) current equation. Secondly, permeability of sodium channels is taken as 15×10^{-12} cm³/s instead of 3.52×10^{-12} cm³/s because after this alteration the developed model is able to produce repetitive firing on sustained depolarization of cell membrane. Dimensions of the cell membrane were not given in the work of Schwarz *et.al.* [16] so area of the cell membrane is taken as 50μm² in accordance with the work of Wesselink *et.al.* [17] who used the model parameters that was given by Schwarz *et.al.* [16]. After the sodium channel permeability alteration, maximum sodium conductance for 50 μm² cell membrane is found as 5120 nS after the linear fit of ohmic relation to GHK relation. The electrophysiological properties of cell membrane are as follows: E_{Na}, sodium reversal potential is 45.4 mV; E_K, potassium reversal potential is -84 mV; $E_{leakage}$, reversal potential for leakage channels is -84 mV. $\overline{g_{Na}}$, maximum sodium channel conductance for 50 μm² membrane is 5120 nS; $\overline{g_K}$, maximum potassium channel conductance for 50 μm² membrane is 30 nS; $\overline{g_{leakage}}$, maximum leakage channel conductance for 50 μm² membrane is 30 nS; c_m, membrane capacitance for 50 μm² membrane is 1.4 pF. Finally, the dynamics of the activating and inactivating gates of sodium channels are doubled to decrease the width of the action potential. The dynamics of ion channels are given in Eqs. 2-4 as

$$\frac{dn}{dt} = \alpha_n(1-n) - \beta_n n, \ n(0) = 0.2563 \quad (2)$$

$$\frac{dm}{dt} = \alpha_m(1-m) - \beta_m m, \ m(0) = 0.0382 \quad (3)$$

$$\frac{dh}{dt} = \alpha_h(1-h) - \beta_h h, \ h(0) = 0.6986 \quad (4)$$

where forward and backward rate constants have the following forms

$$\alpha_n = \frac{0.00798 \times (E_M + 93.2)}{1 - \exp((-93.2 - E_M)/1.10)} \quad (5)$$

$$\beta_n = \frac{0.0142 \times (-76 - E_M)}{1 - \exp((E_M + 76)/10.5)} \quad (6)$$

$$\alpha_m = \frac{3.72 \times (E_M + 18.4)}{1 - \exp((-18.4 - E_M)/10.3)} \quad (7)$$

$$\beta_m = \frac{0.172 \times (-22.7 - E_M)}{1 - \exp((E_M + 22.7)/9.16)} \quad (8)$$

$$\alpha_h = \frac{0.0672 \times (-111 - E_M)}{1 - \exp((E_M + 111)/11)} \quad (9)$$

$$\beta_h = \frac{4.6}{1 + \exp((-28.8 - E_M)/13.4)} \quad (10)$$

All rate constants are in ms⁻¹ and E_M is the membrane voltage. Currents through sodium, potassium and leakage channels are given as

$$I_{Na} = m^3 h \overline{g_{Na}}(E_M - E_{Na}) \quad (11)$$

$$I_K = n^4 \overline{g_K}(E_M - E_K) \quad (12)$$

$$I_{leakage} = \overline{g_{leakage}}(E_M - E_{Leakage}) \quad (13)$$

respectively and they are in pA.

3.2 Model of Fibers

For the model of the fibers compartmental modeling is used [18]. In this modeling strategy, the structure is divided into parts which are homogeneous in themselves. The myelinated fiber consists of nodal part, which is the excitable part, and paranodal part, which is the non-excitable part. Excitable part is modeled as a Hodgkin-Huxley type membrane whereas paranodal part is modeled as a passive RC circuit. Circuit diagram of myelinated fiber is given in Fig 3.
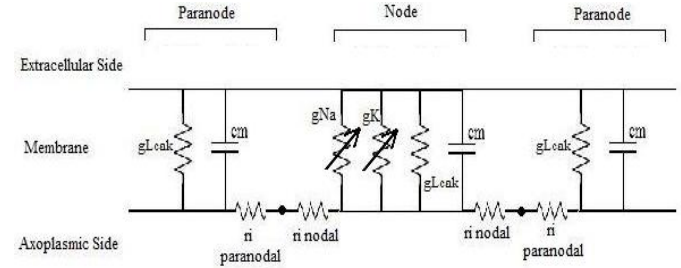
Fig 3. Circuit diagram of myelinated fiber.

Unmyelinated fiber is modeled with only nodal parts since there is no myelination and the fiber is homogeneous in structure. Membrane parameters for nodal and paranodal parts and the intra-axonal resistance is given in Table 1. Cm is the specific membrane capacitance, Rm is the specific membrane resistance and Ri is the intra-axonal resistance.

Table 1. Membrane parameters.

	Cm (F/m²)	Rm (Ω.m²)	Ri (Ω.m)
Nodal part of myelinated fiber	0.028	0.0017	1.25
Paranodal part of myelinated fiber	0.00008	4.25	1.25
Unmyelinated fiber	0.028	0.0017	1.25

The diameter of the axon is chosen as 10 μm for myelinated fiber and the fiber diameter is chosen as 15 μm which is the sum of axon diameter and myelin sheath thichness. With these dimensions length of the nodal part is found as 1.59 μm for myelinated fiber. Length of the paranodal part is chosen as 5000 μm and it is composed of five identical compartments. Only nodal part is excitable, which means that only nodal part contains voltage gated ion channels. Diameter of the unmyelinated fiber is 1.5 μm and length of every

compartment is 100 μm. Both of the fibers has a total length of 1cm.

3.3 Model of Synaptic Transmission

Synapse between neurons is modeled as two independent tanks [19] and it is shown in Fig.4. First tank represents the synaptic vesicle pool that contains the chemical neurotransmitters by which electrical signal conveys from one neuron to the other by chemical means. Height of the liquid in Tank 1 is taken as constant which means that neurotransmitter reserve in the pre-synaptic neuron does not deplete. Resistance of Tank 1 is dependent on pre-synaptic voltage in a way that as the membrane voltage is at its resting potential, resistance is infinite and there is no flow, but when the membrane voltage rises, resistance drops and it reaches a minimum when membrane voltage is at the peak of an action potential. Resistance of Tank 2 is constant and it represents all of the processes in which neurotransmitters diffuse out of the synaptic cleft. Height of the liquid in Tank 2 is analog to the concentration of neurotransmitter in the synaptic cleft.
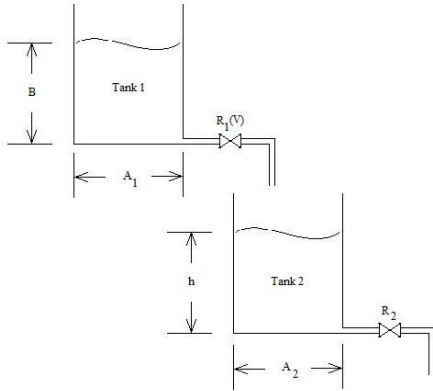
Fig.4. Two tank system for the model of synapse.

The transfer function between the inflow to Tank 2 and the height of the liquid in the same tank is found as in Eq. 2.

$$G_p = \frac{R_2}{A_2 R_2 s + 1} \qquad (14)$$

R_2 is the steady state gain and $A_2 R_2$ is the time constant of the synapse. Time constants for both excitatory and inhibitory transmitters are chosen as 2.5 ms and steady state gain is taken as 5.

Dynamics of post-synaptic neurotransmitter receptors are modeled as first order reaction kinetics and they have two states as particles of voltage gated channels. For excitatory synapses forward rate constant is 2 ms^{-1}mM^{-1} and backward rate constant is 1 ms^{-1} whereas for inhibitory synapses forward rate constant is 0.5 ms^{-1}mM^{-1} and backward rate constant is 0.1 ms^{-1} [20]. Reversal potential is 0mV for excitatory synapses and -90 mV for inhibitory synapses.

3.4 Morphometric Analysis of Component Neurons

For transmission cell, fusiform cell that is given as a 3D reconstruction in part A of Fig.12 in the work of Prescott and

De Koninck [8] is used. For interneuron, islet cell that is given in part B2 of Fig.1 in the work of Melnick [21] is used.

The overall model is completed by cascading the fiber models, synapse model and interneuron and transmission cell models.

4. RESULTS

Response of the developed single excitable cell model for a current pulse stimulus which has a pulse width of 0.0005 ms and amplitude of 3150 pA is shown in Fig.5. The generated action potential is well in accordance with the experimentally recorded one as in [16]. Upon sustained depolarization, model generates multiple action potentials as expected. When the intensity of the stimulus is increased the firing frequency increases, so that the intensity information is coded as the firing frequency. Model also predicts depolarization block which is because of the incomplete opening of inactivation sodium gates after repolarization phase of the action potential.

Due to depolarization block, after the first action potential amplitudes of the following action potentials decrease. Also the model can summate two sub-threshold inputs temporally which is a property of real neurons.

Saltatory conduction is observed in myelinated fiber as expected. The reason for saltatory conduction is that only in nodal parts action potentials are generated and signal is transported through paranodal parts with some attenuation. Conduction along myelnated fiber is shown in Fig.6. On the other hand, signal propagates along unmyelinated fiber passively. When a compartment fires an action potential, this depolarization triggers the adjacent compartment to generate an action potential. So from any part of the unmyelinated fiber action potentials can be recorded whereas in myelinated fiber, only from nodal parts action potentials can be recorded. Propagation of action potentials along unmyelinated fiber is shown in Fig.7. For clarity only responses of two nodal parts are shown. The phase delay due to the transport of the signal from node to node can be seen clearly.
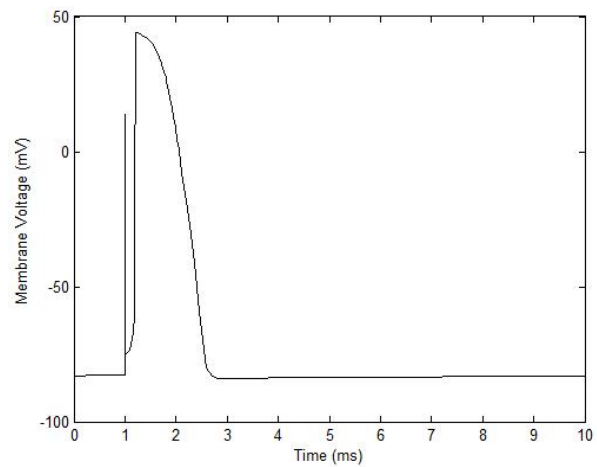
Fig.5. Generated action potential with the model.
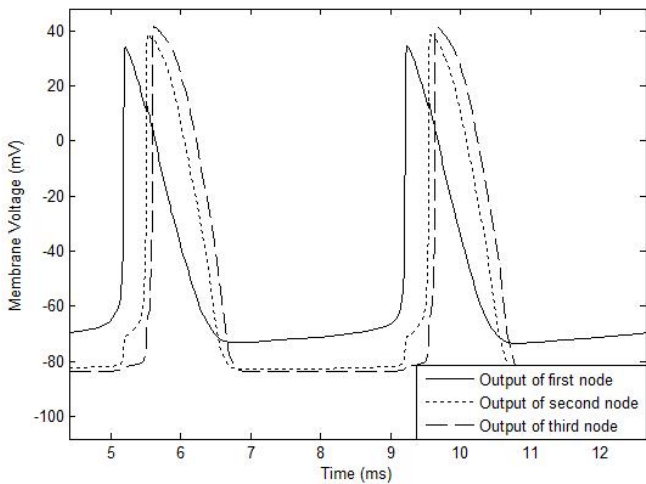
Fig.6. Conduction along myelinated fiber.
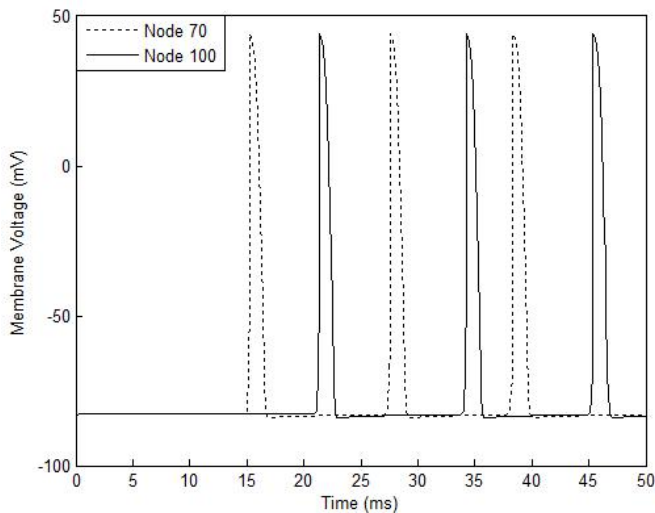
Fig.7. Conduction along unmyelinated fiber.

Conduction velocity in unmyelinated fiber is found as 0.43 m/s and in myelinated fiber velocity is found as 64.35 m/s. Input current intensity- frequency relations of both of the fibers reveal that threshold for conduction along unmyelinated fiber is higher in comparison to myelinated fiber. This is in accordance with everyday experience; light pressure on the skin only produces sensation of touch, however, if the pressure is increased, pain is felt since unmyelinated fibers start to conduct nociceptive signals.

Synapse model predicts two important things; one is the accumulation of neurotransmitter molecules in the synaptic cleft and the other is the tetanization which is the saturation of neurotransmitter concentration in the cleft. With every incoming action potential to the pre-synaptic terminal, neurotransmitter molecules are secreted into the synaptic cleft. If the frequency of action potentials is high enough, neurotransmitter molecules accumulate in the cleft. But this accumulation is not unlimited, the concentration saturates at a level. For two different time constants both of these properties can be observed in Fig.8.
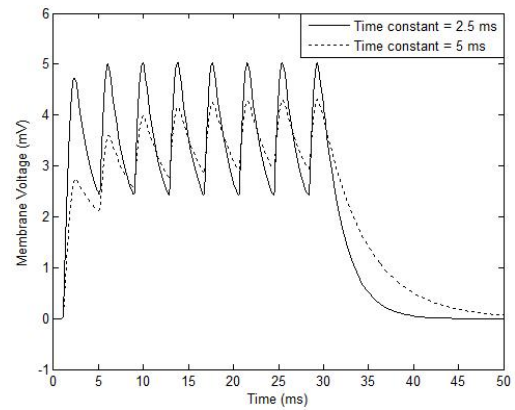
Fig.8 Neurotransmitter concentration in the synaptic cleft.

With the combination of the separate models of the components, gate control structure is built. Structure is tested for different configurations and here two of them will be given. When the myelinated fiber is dissected, since the inhibition effect of the interneuron is decreased, transmission cell fires multiple action potentials as in Fig.9. However, instead of myelinated fiber, if the unmyelinated fiber is dissected, output of the transmission cell is only one action potential so the transmission cell is inhibited to a greater extent. This is shown in Fig.10. In [4] it is stated that stimulation of small diameter fibers, which include C fibers, elicit pain. In addition it is stated that stimulation of large diameter fibers, which include Aβ fibers, may increase pain transiently but reduce it eventually. So except transient effect of large diameter fibers, the whole model predicts the expected outcomes of the gate control theory.

5. CONCLUSIONS

In this study, mathematical model of gate control theory is done. For this purpose, single excitable cell modeled is developed. It is seen that this model can predict depolarization block. With this building block, two fibers, one is myelinated and one is unmyelinated are modeled and the conduction velocities of signlas along these fibers are found to be in physiological ranges. Finally the whole gate control structure is tested for two different configurations and the model can predict the expected outcomes of the gate control theory.
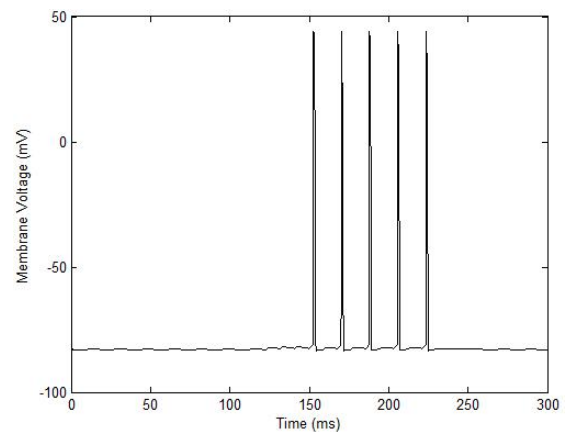
Fig.9. Mylinated fiber is dissected.
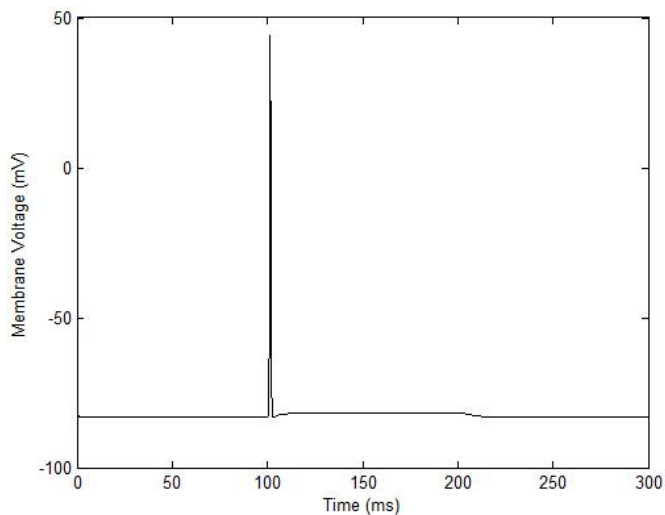
Fig.10. Unmyelinated fiber is dissected.

REFERENCES

[1] M. Stojanovic, "Stimulation methods for neuropathic pain control", *Current Pain and Headache Reports*, vol. 5, no. 2, pp. 130-137, 2001.

[2] B. Graham, A. Brichta, and R. Callister, "Moving from an averaged to specific view of spinal cord pain processing circuits", *Journal of Neurophysiology*, vol. 98, pp. 1057-1063, 2007.

[3] N. Britton and S. Skevington, "A mathematical model of the gate control theory of pain", *Journal of Theoretical Biology*, vol. 137, no. 1, pp. 91-105, 1989.

[4] M. Haeri, D. Asemani, and S. Gharibzadeh, "Modeling of pain using artificial neural networks", *Journal of Theoretical Biology*, vol. 220, no. 3, pp. 277-284, 2003.

[5] R. Melzack and P. Wall, "Pain mechanisms: a new theory", *Science*, vol. 150, no. 3699, pp. 971-978, 1965.

[6] E. Kandel, J. Schwartz, and T. Jessell, *Principles of Neural Science*. Appleton & Lange, 2000.

[7] P.Wall, "The gate control theory of pain mechanisms", *Brain*, vol. 101, no. 1, pp. 1-18, 1978.

[8] S. Prescott and Y. Koninck, "Four cell types with distinctive membrane properties and morphologies in lamina I of the spinal dorsal horn of the adult rat", *The Journal of Phynsiology*, vol. 539, no. 3, pp. 817-836, 2002.

[9] T. Grudt and E. Perl, "Correlations between neuronal morphology and electrophysiological features in the rodent super_cial dorsal horn", *The Journal of Physiology*, vol. 540, no. 1, pp. 189-207, 2002.

[10] Y. Lu and E. Perl, "Modular organization of excitatory circuits between neurons of the spinal super_cial dorsal horn (laminae I and II)", *The Journal of Neuroscience*, vol. 25, no. 15, pp. 3900-3907, 2005.

[11] L. Almarestani, S. Waters, J. Krause, G. Bennett, and A. Ribeiro-da Silva, "Morphological characterization of spinal cord dorsal horn lamina I neurons projecting to the parabrachial nucleus in the rat", *The Journal of Comparative Neurology*, vol. 504, pp. 287-297, 2007.

[12] Z. Han, E. Zhang, and A. Craig, "Nociceptive and thermoreceptive lamina I neurons are anatomically distinct", *Nature Neuroscience*, vol. 1, no. 3, pp. 218-225, 1998.

[13] A. Todd and J. McKenzie, "GABA-immunoreactive neurons in the dorsal horn of the rat spinal cord", *Neuroscience*, vol. 31, no. 3, pp. 799-806, 1989.

[14] D. Maxwell, M. Belle, O. Cheunsuang, A. Stewart, and R. Morris, "Morphology of inhibitory and excitatory interneurons in super_cial laminae of the rat dorsal horn", *The Journal of Physiology*, vol. 584, no. 2, pp. 521-533, 2007.

[15] A. Hodgkin and A. Huxley, "A quantitative description of membrane current and its application to conduction and excitation in nerve", *J. Physiol. (Lond.)*, vol. 117, pp. 500-544, 1952.

[16] J. Schwarz, G. Reid, and H. Bostock, "Action potentials and membrane currents in the human node of Ranvier", *Pflügers Archiv European Journal of Physiology*, vol. 430, no. 2, pp. 283-292, 1995.

[17] W. Wesselink, J. Holsheimer, and H. Boom, "A model of the electrical behavior of myelinated sensory nerve fibres based on human data", *Medical and Biological Engineering and Computing*, vol. 37, no. 1, pp. 228-235, 1999.

[18] C. Koch and I. Segev, Methods in neuronal modeling: from ions to networks. The MIT Press, 1998.

[19] G. Stephanopoulos, *Chemical process control: an introduction to theory and practice*, Prentice-Hall Englewood Cliffs, 1984.

[20] A. Destexhe, Z. Mainen, and T. Sejnowski, "An effcient method for computing synaptic conductances based on a kinetic model of receptor binding", *Neural Computation*, vol. 6, no. 1, pp. 14-18, 1994.

[21] I. Melnick, "Morphophysiologic properties of islet cells in substantia gelatinosa of the rat spinal cord", *Neuroscience Letters*, vol. 446, no. 2-3, pp. 65-69, 2008